2021 IEEE/RSJ International Conference on Intelligent Robots and Systems (IROS)
September 27 - October 1, 2021. Prague, Czech Republic

Multi-Stage Energy-Aware Motion Control with Exteroception-Defined Dynamic Safety Metric*

Kirill Artemov[1], Sergey Kolyubin[1], Stefano Stramigioli[1,2]

***Abstract*— We address the problem of motion control for safe physical interaction, and in particular finding new ways for impedance controller parameters' adaptation to ensure better safety with minimum possible lose in robot performance. We propose an exteroception-based dynamically updated safety metric that takes into account current robot state and inertia as well as external objects' mass, shape, material properties, velocity, sensor confidence and existing sampling rates. We also present how this metric can be applied to design a finite state machine of the multi-stage controller, which allows us to prioritize either safety of performance by setting different energy and power constraints with smooth transition in between free motion and interaction modes.**

Compliance and Impedance Control; Safety in HRI; Sensor-based Control

I. Introduction

Collaborative robots are designed specifically to perform tasks in a shared workspace with human and even assist each other, which involves multiple scenarios of physical Human-Robot Interaction (pHRI). Therefore, protecting human from possible injuries that a moving robot can inflict becomes a top priority and a very active research field [1].

General safety requirements for collaborative robots and the quantitative safety assessments of pHRI are available in ISO 10218-1:2011 and ISO/TS 15066:2016 standards.

In reality, different collision scenarios can occur. The most common safety metric for robots is the Head Injury Criteria (HIC), which evaluates the effect of acceleration during a contact on the head, but it does not always reflect the actual safety of the robot [2]. For the analysis of head injuries (concussion), a power-based safety metric Head Impact Power (HIP) has been introduced in [3]. For neck contact safety analysis, force-based metrics are also used in [4]. Bone fracture safety analyzes are performed using energy-based metrics in [5]. Hence, two bottlenecks can be seen: (1) there are different metrics for different parts of the human body, (2) all metrics don't depend on information about the environment.

As it's illustrated in Fig. 1, the types of collisions significantly can depend on a shape, a material and an interaction type, as well as a relative velocity and colliding objects mass. Thus, preventing injury can only be achieved by ensuring that multiple safety criteria are met [6]–[9].

*This work is supported by the Russian Science Foundation grant (project №17-79-20341).

[1]*Biomechatronics and Energy-Efficient Robotics Lab, ITMO University, St. Petersburg, Russia*
[2]*Department of Electrical Engineering, Mathematics and Computer Science, University of Twente, The Netherlands* {kaartemov, s.kolyubin}@itmo.ru

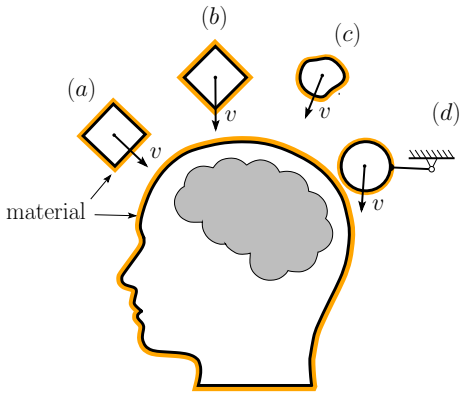

Fig. 1. Cases of possible collisions with: (a) blunt object, (b) sharp object, (c) soft object, (d) tangential collision (friction burn)

Specifically, possible injures happen due to high momentum transferred by the robot to operators' body parts during collision [10], [11]. Therefore, natural ways to improve pHRI safety are either to limit robot maximum energy, power, acceleration, force, momentum, and others or make the robot softer such that it will dissipate most of the impact energy inside its structure.

This task sparked research on elastic actuation. Providing this property at the hardware level allows to resolve a possible collision between digital world of control systems and continuous robot dynamics, since mechanics provides us infinite bandwidth. Many fruitful results on Variable Stiffness Actuators/Variable Impedance Actuation (VSA/VIA) design have been achieved in the past decade, e.g. [12], [13]. There are also elegant and physically-consistent control policies that balance injected and dissipated energy [14], [15].

However, despite all these achievements, tightening energy and power constraints and making robots softer may result in decrease of robot operation speed, stability, accuracy, and payload capacity. A promising approach to make safety-implied limitations more flexible is to include extra sensory inputs in the decision-making loop.

It has straight analogy with how we or others leaving creatures move. A robot using only interoceptive sensors is like a human walking or manipulating objects in unknown surroundings blindfolded. Movements will be slow and inaccurate with small muscular pre-tension to minimize effect of possible bumps. However, if the robot is given "eyes" like a human in a well-lit room, it will be fast, more precise, and able to predict a possible collision with an unexpected obstacle and react in advance.

A general framework of how such approach can be success-

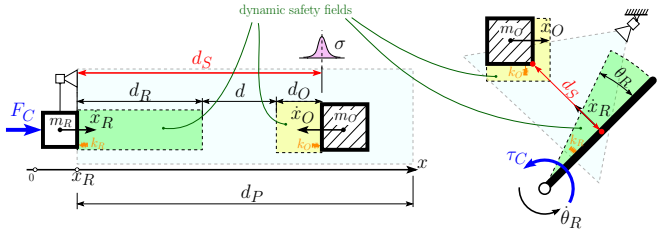

(a) Translation joint (b) Rotation joint

Fig. 2. Dynamic safety metric for 1-DOF example: (a) translation joint, (b) rotation joint

fully implemented for industrial robot motion planning and control systems, specifically for online trajectory generation, to make it more intelligent in reacting to unforeseen events was described, e.g. in [16].

The contribution of this work is *a multi-stage energy-aware control schema*, where the switching proposed is using an *exteroception-defined dynamic safety metric*.

Dynamic safety metric is a value that is calculated to check if the robot is still moving within the *dynamic safety field* (green and yellow in Fig 2). *Dynamic safety field* or "Safety Bubble" is an area around a robot body where it can move safely without the risk of possible collisions.

II. General Framework

Here we briefly describe main features of the proposed control strategy and refer to related studies to highlight our contribution.

A. Dynamic Safety Fields ("Safety Bubble")

Exteroceptive sensors like cameras, lidars, range finders, etc. make it possible to define a specific area around the robot. This information can be used to calculate the distance to possible collision. A corresponding idea of *dynamic safety fields* was proposed in [17]. The safe operation distance for a mobile manipulator motion is updated there continuously based on robot's current velocity. We take this idea further and propose a comprehensive framework.

In this paper, we suggest to define a safety field's shape and dimensions from the condition of guaranteeing a complete stop or slowing-down to a pre-defined safe velocity inside this "bubble", taking into account not only robot's and obstacle's state and properties (tensor of inertia, mass, shape, material stiffness, etc.), but also digital control system and sensor properties such as sampling rate and confidence. See Fig. 2 for illustration on suggested safety field calculation approach.

B. Multi-Stage Control

There are different ways to decompose a robot's movement within physical interaction scenarios into stages. In [18], the authors propose to divide the robot's movements into three phases: pre-impact, impact, and post-impact. In [19] the authors summarized previous studies and proposed to decompose any robot movements into seven elementary phases from pre-collision to reaction and post-collision. Switching between these stages can be organized using finite state machines (FSM) concept similar to [20].

Accordingly, different control strategies can be implemented across defined stages to guarantee safe physical interaction. For example, in [21], the authors presented a reactive obstacle avoidance approach during physical contact, while a displacement of the trajectory reference is computed to reduce the interaction force and move in the direction of avoidance (around) the obstacle. In [14], the impedance control approach was proposed, where stiffness and damping parameters were adjusted according to energy- and power-based safety metrics. Further, in [15], this approach was generalized to a multidimensional system. These works focus on the robot behavior at the phase, when unexpected collision has already occurred.

In our study we suggest to decompose the robot's movement into three stages based on the *dynamic safety metric* that were introduced before. The *Stage I* is a "free movement", while obstacles are far away for collision and we prioritize performance by applying weak safety constraints. The *Stage II* is a "collision expected", where we start applying more conservative safety limits that change proportionally to the distance-to-collision to avoid possible impact or make it a "soft landing". The *stage III* is a 'at contact', where we prioritize safe interaction over performance indicators of, e.g. trajectory tracking. Fig. 3 illustrates the proposed stages' decomposition scheme.

Control algorithms for stages I and III are based on those proposed in [15] with some modifications. For *Stage II* we propose a novel control strategy, where controller compliance and damping coefficients are adjusted in accordance with introduced *dynamic safety metric*.

III. Safety Metric Calculation from Exteroception Data

A. Model for illustrative 1-DOF example

For illustrative purposes we consider a 1-DOF example to describe all features and steps of the proposed approach intuitively. All presented results can be generalized to 6-DOF spatial motion similar to how it was done in [15].

Let's a 1-DOF robot be modeled as a body of a constant mass m_R and (material) stiffness k_R moving with velocity $\dot{x}_R(t)$ on the left and an object of possible collision that can be a human or any surrounding object (further denoted as 'an obstacle') modeled as a body with a constant mass m_O and (material) stiffness k_O moving with velocity $\dot{x}_O(t)$ on the right (see Fig. 2). The robot is equipped with an exteroceptive sensor that measures the distance to an obstacle d_S, and the field of view of the sensor is d_P.

According to the 2nd Newton's law, the equation of motion of our robot can be written as

$$m_R \ddot{x}_R(t) = F_C(t) + F_I(t), \tag{1}$$

where F_C and F_I are control and interaction forces respectively.

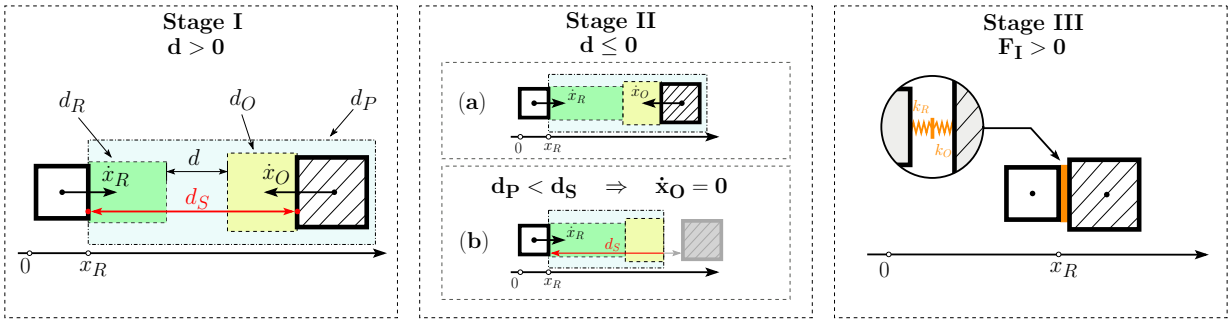

Fig. 3. Diagram of motion stages

According to the Hooke's law, the interaction force could be modeled as

$$F_I(t) = \begin{cases} 0, & x_R(t) \le x_O(t), \\ k_m\big(x_R(t) - x_O(t)\big), & otherwise, \end{cases} \tag{2}$$

where $x_O(t)$ and $x_R(t)$ are the obstacle's and the robot's coordinate respectively[1], and the aggregated material stiffness can be calculated based on the formula for series connection of two (robot's and obstacle's) 'springs'

$$k_m = \left(\frac{1}{k_R} + \frac{1}{k_O}\right)^{-1}. \tag{3}$$

Throughout the paper we implement impedance control. Thus, the control force is calculated as

$$F_C(t) = k(t)\big(x_V(t) - x_R(t)\big) - b(t)\dot{x}_R(t) \tag{4}$$

such that we can shape the closed-loop system behavior by three control parameters, namely controller stiffness k (proportional gain), controller damping b (derivative gain), and a virtual spring suspension point coordinate x_V (virtual position).

The total energy of the robot will be [15]

$$E_{tot}(t) = \frac{1}{2} m_R \dot{x}_R^2(t) + \frac{1}{2} k(t)\big(x_V(t) - x_R(t)\big)^2. \tag{5}$$

At the same time, the output power of the controller can be written as

$$P_c(t) = \big(k(t)(x_V(t) - x_R(t)) - b(t)\dot{x}_R(t)\big)\,\dot{x}_R(t). \tag{6}$$

B. Robot's "Safety Bubble"

The trigger that is used for switching between *Stage I* and *Stage II* (see Fig. 3) is the safety metric dynamically updated at each discrete instant of time t_k ($k = 0, 1, 2, \ldots$) with a constant sampling $\tau_r = t_{k+1} - t_k$

$$d(t_k) = \bar{d}(t_k) - \big(d_R(t_k) + d_O(t_k)\big), \tag{7}$$

where $\bar{d}(t_k) = \min\{d_S(t_k), d_P\}$, $d_S(t_k)$ is a sensor measurements, d_P is a maximum perception distance, $d_O(t_k)$ is the size of safety field around the obstacle, and $d_R(t_k)$ is the distance that is needed for safe stop if rapid braking was applied.

[1]Positive value of $\big(x_R(t) - x_O(t)\big)$ means that two bodies are in contact.

Here we explain how all variables in (7) should be calculated for a given example, and start from deriving relations for the safety distance from the robot side d_R.

The idea behind defining the robot's "safety bubble" is that its size should be enough for the robot to stop inside it before collision with an object by applying rapid braking, which is described below.

Let's describe the robot's state at time t_k by its current velocity $\dot{x}_{R,0} = \dot{x}_R(t_k)$ and coordinate $x_{R,0} = x_R(t_k)$.

Remark 1. Since we estimate the safety distance along the direction of current motion, the relation $\dot{x}_{R,0} \ge 0$ will be valid for further calculations.

An actuator of a real robot has constraints on a maximum force $|F_C| \le F_m$ ($F_m > 0$), therefore the maximum acceleration $|\ddot{x}_R(t)| \le a_m$ for a known mass m_R equals

$$a_m = \frac{F_m}{m_R}. \tag{8}$$

To reduce possible jumps in control, we avoid maximum deceleration force to be applied instantly and instead assign it as linearly changing in time. Therefore, we also set the maximum jerk $|\dddot{x}_R(t)| \le j_m$ ($j_m > 0$).

As the result, possible velocity, acceleration, and jerk profiles for rapid braking are depicted at Fig. 4, and its analytical expressions can be easily derived from kinematics relations.

Also, for the rapid breaking time t_b taking into account the sampling time of the robot's digital controller T_R, which is assumed to be constant, the integer number of sampling

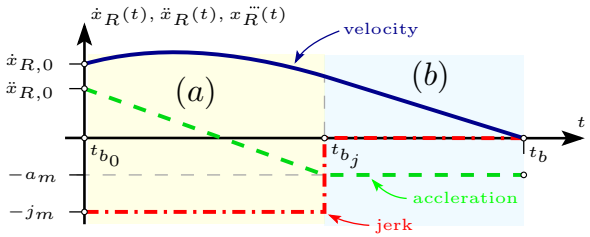

Fig. 4. Robot's velocity, acceleration, and jerk profiles for rapid braking. (a) is a constant jerk motion, (b) is a uniformly accelerated motion.

intervals should be used:

$$n_b = \text{ceil}\left(\frac{t_b - t_{b_0}}{T_R}\right), \quad n_{b_j} = \text{ceil}\left(\frac{t_{b_j} - t_{b_0}}{T_R}\right), \quad (9)$$

where $\text{ceil}(\cdot)$ is the round-up function, t_{b_0} and t_{b_j} are rapid breaking time variables.

Based on the introduced notation, the distance $d_R(t_k)$ can be easily calculated using classical uniform motion equations.

Remark 2. To compute $d_R(t_k)$ the relative velocity value $\dot{x}(t_k)$ can be used. It is easier to calculate it from exteroceptive sensing than calculating the obstacle's velocity itself. For example, one can use computer vision and numerically differentiate relative change in coordinates between two moving frames or do the same for range measurement between the robot and an obstacle.

Remark 3. The safety distance from the robot side $d_R(t_k)$ actually depends on a set of various parameters, namely robot mass m_R, existing force F_m and jerk j_m constraints, robot's current velocity $\dot{x}_R(t_k)$ and acceleration $\ddot{x}_R(t_k)$, as well as controller sampling time T_R.

C. Obstacle's "Safety Bubble"

The next component in (7) is $d_O(t_k)$, which defines the size of the "safety bubble" around an obstacle. Fig. 5 illustrates some examples of how these "safety bubble" can be assigned.

In general, $d_O(t_k)$ calculation should be reasoned by impact modelling, e.g. equations for resulting velocities, aggregate momentum, and energy exchange [22]. Below are some arguments in compact formulation that help us distinguish between different collision types (see Fig. 1) should be considered: (1) collision with a heavier object lead to higher normal impulse $S = (1 + K_r)\frac{m_R m_O}{m_R + m_O}\dot{x}$; (2) material defines restitution and stiffness coefficients K_r and k_O respectively. The higher value k_O leads to harder impacts; (3) contact with sharp edges lead to deeper penetration at impact, therefore we should increase d_O directly proportional to the obstacle's shape curvature C_r (calculated locally for the possible collision area); (4) by tracking robot and obstacle relative motion, we can estimate relative velocity $\dot{x}$ and meeting angle ϕ (angle between motion directions of two colliding objects). Based on that we can distinguish between, e.g. frontal collision ($\phi = \pi$) and shear impact ($\phi = \pi/2$).

According to a sample-and-hold approach, aforementioned estimates are constant for $t \in [t_h, t_h + T_s)$, where T_s is exteroceptive sensor's sampling interval. The higher it is, the more uncertainty in measurement we have.

Finally, a general expression for the obstacle's "safety bubble" can be written as

$$d_O(t_k) = K_m(m_O)K_C\big(C_r(t_h)\big)K_a \sin\left(\phi(t_h) - \frac{\pi}{2}\right) \cdot \\ \cdot K_s(k_O)K_v\big(\dot{x}(t_h)\big)K_t(T_s)\bar{d}_O, \quad \forall t_k \in [t_h, t_h + T_s) \quad (10)$$

where $\bar{d}_O > 0$ is the minimum constant "safety bubble" size and $K_{(\cdot)}(\cdot)$ are monotonically increasing functions $\min_x K_{(\cdot)}(x) = 1$.

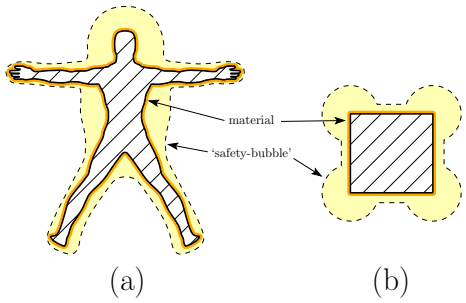

Fig. 5. Obstacle's "safety bubble": (a) a human, (b) a rigid box

D. Taking into account sensor confidence

The remaining two metrics in (7) are related to the distance between the robot and an obstacle estimated from exteroception.

By d_P we define the constant maximum perception distance at which an obstacle can be recognized by the sensor. This parameter should be defined by the developer in advance, given sensor specifications.

Remark 4. If we can not recognize an obstacle within the maximum perception distance, i.e. for ($d_P \leq d_S$), then we set all parameters in (10) to its nominal values and assign in the calculation distance $d_R\ \dot{x}(t_k) = \dot{x}_R(t_k)$.

The actual distance between the robot and an obstacle d_S (for $d_P > d_S$) is estimated from corrupted (by noise) sensory signals. We assume that measurements' noise obey normal distribution. Then, the following expression for d_S calculation can be used

$$d_S(t_k) = \bar{d}_S(t_k) - 3\sigma(t_k), \quad \forall t_k \in [t_h, t_h + T_s) \quad (11)$$

where $\bar{d}_S$ is the distance mean value calculated from filtered measurements and σ is the standard deviation that can be estimated from a moving variance with a directional window of size l. The directional window includes the current distance measurement at t_h and t_{h-1}, $t_{h-2}, \ldots, t_{h-l}$ measurements before. Here we add three sigma to guarantee that the estimated distance value is not bigger than the actual distance to the obstacle with a 99.7% probability.

IV. Multi-Stage Energy-Aware Control Algorithm

The proposed multi-stage control scheme always takes into account the energy of the robot to ensure maximum safety in any operating modes.

A. Stage I: Free Motion

At this stage we apply an energy-aware control strategy similar to [14], but prioritize robot performance while setting maximum allowed energy limits.

In free motion when safety bubbles intersection is not detected ($d(t_k) > 0$) we adapt the stiffness coefficient of the impedance controller (4) as

$$k(t) = \begin{cases} k_M, & E_{tot}(t_k) \leq E_{max}, \\ \dfrac{2E_{max} - m\,\dot{x}_R^2(t_k)}{(x_V(t_k) - x_R(t_k))^2}, & \text{otherwise}, \end{cases} \quad (12)$$

where $t \in [t_k, t_{k+1})$, $k_M > 0$ is the nominal stiffness value.

Remark 5. Weak constraints on E_{max} should be set by the developer on basis of risks. For example, selected E_{max} should guarantee that $d_R(t_k) < d_P$ for all $t_k > 0$. Also, E_{max} can be interactively adjusted based on surroundings' analysis and set to a lower value if exteroception data says that the robot's environment became highly cluttered. It will allow to avoid frequent switching between stages I and II and thereby to lower energy losses because of acceleration and braking. Since these values are set, the following condition must be met: $\frac{1}{2} m_R x_V^2 < E_{max}$.

For better precision and dynamic performance measures of robot control (less undesired oscillations), at this stage we adjust damping coefficient in (4) such that our robot behaves as a critically damped system

$$b(t) = b(t_k) = 2\sqrt{m_R\, k(t_k)}, \quad t \in [t_k, t_{k+1}) \tag{13}$$

which guarantees damping ratio $\xi = 1$.

B. Stage II: Collision Expected

Knowing the distance to the nearest obstacle $d_{R,0} = d_S = d_R + d_O$, the robot's current total energy E_{tot} and its corresponding limitations for safe interaction E_{SAFE}, and assigning a desired deceleration force profile $F_{C_p}(t_k)$ we can further derive rules for the impedance controller parameters adaptation at the braking stage.

To slow-down the robot, we have to dissipate a certain amount of total energy by applying the corresponding control force:

$$\Delta E = E_{tot} - E_{SAFE} = -\int_{t_0}^{t_0+T} P_C(\tau)\mathrm{d}\tau, \tag{14}$$

where E_{tot} and $P_C(t)$ are calculated from (5) and (6) respectively, T is the complete braking time.

Remark 6. It is clear that we can dissipate energy by increasing damping coefficient $b(t)$ ("virtual friction") simultaneously decreasing "virtual spring" stiffness $k(t)$.

If we set a trapezoid deceleration force profile (see Fig. 6) with a desired maximum braking force value $F^*_{C_p}$ and an initial force value $F_{C_{p0}}$, then we have

$$F^*_{C_p} = -\frac{\Delta E - \frac{1}{2} F_{C_{p0}} d_d}{d_R - d_a - d_d} = a^* m_R, \tag{15}$$

where d_a and d_d can be computed from actuator transient response. For reasons of compactness of the paper, we do not present the derivation of some formulas, but the intuition can be extracted from the explanatory figures.

The new acceleration a^* can then be determined from the expression (15) for a softer deceleration.

Then, from a uniform motion and for the following deceleration time intervals $\Delta t_1, \Delta t_2, \Delta t_3$, the complete breaking time (some as in (14)) $T = \Delta t_1 + \Delta t_2 + \Delta t_3$ and $\Delta_2 = \Delta t_1 + \Delta t_2$

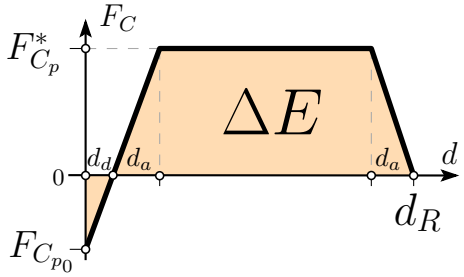

Fig. 6. The force profile to slow-down the robot

the trapezoid profile is written as:

$$F_{C_p}(t_k) = -m_R \begin{cases} j_m t_k - a_0, & 0 \le t_k < \Delta t_1, \\ a^*, & \Delta t_1 \le t_k < \Delta_2, \\ a^* + j_m(\Delta_2 - t_k), & \Delta_2 \le t_k \le T, \end{cases} \tag{16}$$

Thus, for $t \in [t_k, t_{k+1})$ we have the following adaptation for the controller stiffness

$$k(t) = \big(k_0 - k(t_0)\big)\left(\frac{t_k}{T}\right) + k(t_0) \tag{17}$$

and damping

$$b(t) = \frac{k(t)\big(x_V(t_k) - x_R(t_k)\big) - F_C(t_k)}{\dot{x}_R(t_k)}. \tag{18}$$

Remark 7. In practice, on top of (18) we used saturation by hyperbolic tangent function to prevent damping coefficient peaking for $\dot{x}_R(t_k) \approx 0$.

C. Stage III: At Contact

At this stage we implement safety- and passivity-aware controller similar to [14], but in contradistinction to the *Stage I* here we prioritize safety of physical interaction over robot performance and set stronger constraints:

$$E_{tot} < E_{SAFE}, \quad P_c < P_{SAFE}, \tag{19}$$

where $E_{SAFE} < E_{max}$ and $P_{SAFE} < P_{max}$ are boundary values for allowed total energy and controller power respectively.

Thus, for *Stage III* providing a safe amount of energy can be achieved by adjusting the stiffness coefficient in (4) as:

$$k(t) = \begin{cases} k_0, & E_{tot}(t_k) \le E_{SAFE}, \\ \dfrac{2E_{SAFE} - m_R\, \dot{x}_R^2(t_k)}{(x_V(t_k) - x_R(t_k))^2}, & \text{otherwise}, \end{cases} \tag{20}$$

where $t \in [t_k, t_{k+1})$ and $0 < k_0 < k_M$ is the initial constant value.

At the same time, the safety of velocity limiting can be achieved from a controller's power output (6) by adjusting damping coefficient b as:

$$b(t) = \begin{cases} 2\sqrt{m_R k(t_k)}, & P_c(t_k) \le P_{SAFE}, \\ \dfrac{k(t_k)\,(x_V(t_k) - x_R(t_k))\,\dot{x}_R(t_k) - P_{SAFE}}{\dot{x}_R^2(t_k)}, & \text{else}, \end{cases} \tag{21}$$

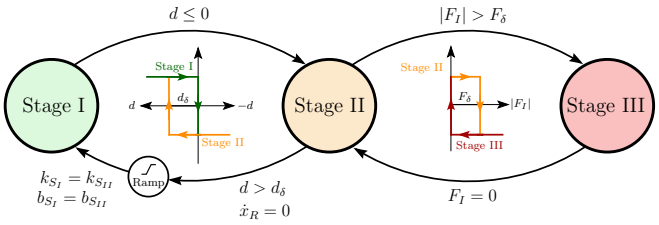

Fig. 7. Finite state machine of the proposed multi-stage controller

where $t \in [t_k, t_{k+1})$ and $b_0 = 2\sqrt{m_R k_0}$ is a critical damping.

Additionally, to ensure stability of physical interaction, we introduce the passivity layer [14] that is based on the energy-tank concept. For one joint is defined as:

$$\begin{bmatrix} \dot{s} \\ \dot{p} \end{bmatrix} = \begin{bmatrix} 0 & u \\ -u & 0 \end{bmatrix} \begin{bmatrix} s \\ \frac{p}{m} \end{bmatrix} \tag{22}$$

where s is state of the storage, p is the momentum of a robot, $\frac{p}{m} = \dot{x}_R$ is the robot velocity, and control transmission ratio u is defined as:

$$u = \begin{cases} 0 & \text{if } \big((H(s) < \epsilon) \wedge (P_c > 0)\big) \\ -\dfrac{F_C}{s} & \text{otherwise,} \end{cases} \tag{23}$$

where F_C is the controller force, $H(s) = \frac{1}{2}s^2$ is energy in the tank, $\epsilon > 0$ is the minimum energy in the tank.

Thus, the resulting relation for the control force will be

$$F_C(t) = -u(t)s(t), \tag{24}$$

where $u(t)$ and $s(t)$ values are defined from (22)–(23).

D. Switching between stages

The last issue in multi-stage controller discussion is the switching policy. We represent the proposed controller as a finite state machine, where transfer between states (stages) is triggered when distance to obstacle d_S and interaction force F_I pass thresholds. The transition conditions can be seen in Fig. 7.

Remark 8. We introduce distance and contact force margins (dead-zones) d_δ and F_δ respectively and hysteresis-like switching between stages to avoid chattering.

V. Validation

To illustrate advantages of the proposed approach, simulation was performed for $m_R = 1$, $x_{R,0} = 0$, $k_m = 100$, $x_V(t) = 2\sin(t)$, $x_O(t) = 2.5 - \sin(t)$. The default controller parameters were used the same for all tests: $k_0 = 100$, $b_0 = 20$. Parameters for Energy- Safety-Aware control (for Stage I and Stage III) was defined as: $E_{max} = 10$, $E_{SAFE} = 1$, $P_{SAFE} = 0.5$, $s(0) = 5$.

Three different approaches was compared: Impedance Controller (IC) with constant stiffness and damping, Energy-Safety-Aware Controller (SEA) from [14] and the proposed multi-stage controller (MSEA). For SEA we set maximum energy and controller power constraints to 3 J and 5 W respectively based on HIC metric [11].

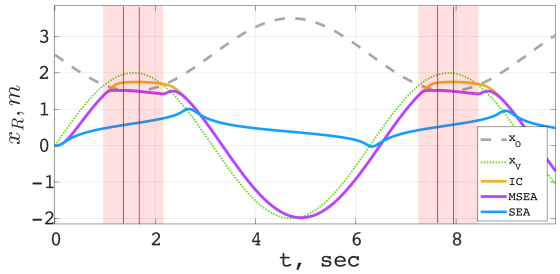

Fig. 8. Robot reference and actual coordinates and obstacle coordinates

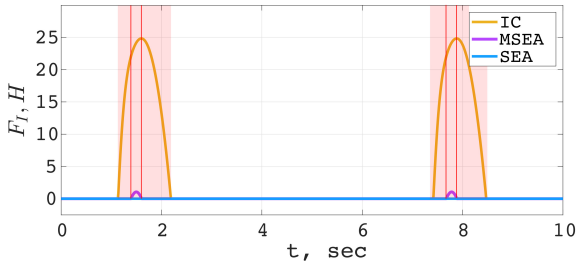

Fig. 9. Interaction force between the robot and a moving obstacle

Simulation results in Figs. 8-12 show that by proposed stiffness and damping adaptation rules we get much better tracking performance compared to SEA and better interaction force control compared to IC. Red rectangles highlight time intervals where MSEA is operating at Stage II, while vertical red lines illustrate time instants, when physical contact between the robot and an obstacle starts and ends. The unsatisfactory performance of SEA on a fast trajectory is associated with hard energy and power constraints.

VI. Conclusions and Future Work

This work illustrates how exteroceptive data can be used to introduce dynamically updated safety metric and organize switching between stages with different impedance controller's stiffness and damping coefficients' adaptation rules. It empowered control algorithms with prediction abilities that allowed simultaneous improvement in safety and performance of robot motion control system by setting weaker safety constraints when possible; lower energy and power limits and energy-tanks when needed for stable physical interaction; and a smooth transition in between these modes.

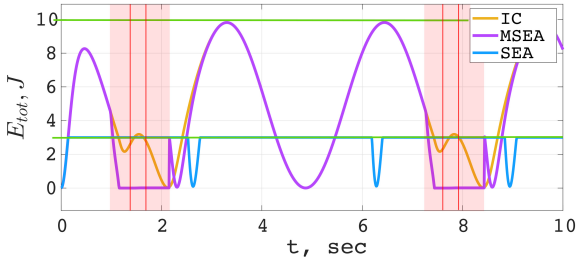

Fig. 10. Total energy in the system (green lines illustrate constraints defined below)

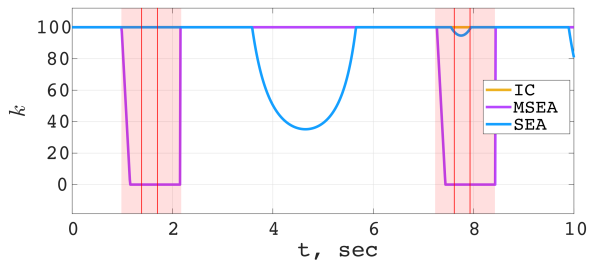

Fig. 11. Stiffness coefficient adaptation

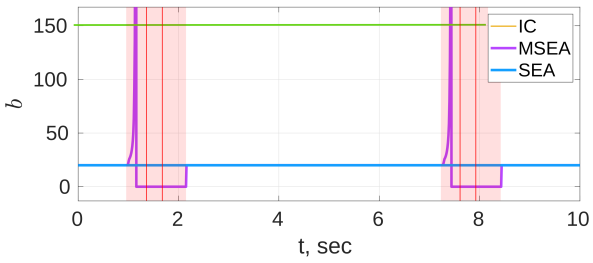

Fig. 12. Damping coefficient adaptation (green line illustrate saturation level)

For the future work we are planning to extended it for multi-DOF cases (that can be done directly similar to [14]), bringing even smarter system behaviour. Indeed, by predicting the direction of possible physical contact, we can coordinate scaling of stiffness and damping coefficients for different motion axes either in configuration or task space, and make system more energy-efficient by routing system energy instead of its dissipation during braking. We also plan to demonstrate how computer vision can be used in practice to extract obstacle properties for "safety bubbles" calculation.

REFERENCES

[1] A. Zacharaki, I. Kostavelis, A. Gasteratos, and I. Dokas, "Safety bounds in human robot interaction: A survey," *Safety science*, vol. 127, p. 104667, 2020.

[2] S. Haddadin, A. Albu-Schäffer, and G. Hirzinger, "Requirements for safe robots: Measurements, analysis and new insights," *The International Journal of Robotics Research*, vol. 28, no. 11-12, pp. 1507–1527, 2009.

[3] J. A. Newman and N. Shewchenko, "A proposed new biomechanical head injury assessment function-the maximum power index," SAE Technical Paper, Tech. Rep., 2000.

[4] K. Ikuta, H. Ishii, and M. Nokata, "Safety evaluation method of design and control for human-care robots," *The International Journal of Robotics Research*, vol. 22, no. 5, pp. 281–297, 2003.

[5] N. Yoganandan, F. Pintar, D. Maiman, J. Cusick, A. Sances Jr, and P. Walsh, "Human head-neck biomechanics under axial tension," *Medical engineering & physics*, vol. 18, no. 4, pp. 289–294, 1996.

[6] M. Wassink and S. Stramigioli, "Towards a novel safety norm for domestic robotics," in *2007 IEEE/RSJ International Conference on Intelligent Robots and Systems*. IEEE, 2007, pp. 3354–3359.

[7] S. Haddadin, A. Albu-Schaffer, M. Frommberger, J. Rossmann, and G. Hirzinger, "The "dlr crash report": Towards a standard crash-testing protocol for robot safety-part i: Results," in *2009 IEEE International Conference on Robotics and Automation*. IEEE, 2009, pp. 272–279.

[8] S. Haddadin, A. Albu-Schäffer, and G. Hirzinger, "Safety analysis for a human-friendly manipulator," *International Journal of Social Robotics*, vol. 2, no. 3, pp. 235–252, 2010.

[9] J. Liu, Y. Yamada, and Y. Akiyama, "Calculating the supplied energy for physical human-robot interaction," in *2021 IEEE International Conference on Intelligence and Safety for Robotics (ISR)*. IEEE, 2021, pp. 157–160.

[10] S. Haddadin, S. Haddadin, A. Khoury, T. Rokahr, S. Parusel, R. Burgkart, A. Bicchi, and A. Albu-Schäffer, "On making robots understand safety: Embedding injury knowledge into control," *The International Journal of Robotics Research*, vol. 31, no. 13, pp. 1578–1602, 2012.

[11] R. Alami, A. Albu-Schäffer, A. Bicchi, R. Bischoff, R. Chatila, A. De Luca, A. De Santis, G. Giralt, J. Guiochet, G. Hirzinger *et al.*, "Safe and dependable physical human-robot interaction in anthropic domains: State of the art and challenges," in *2006 IEEE/RSJ International Conference on Intelligent Robots and Systems*. IEEE, 2006, pp. 1–16.

[12] B. Vanderborght, A. Albu-Schaeffer, A. Bicchi, E. Burdet, D. Caldwell, R. Carloni, M. Catalano, O. Eiberger, W. Friedl, G. Ganesh, M. Garabini, M. Grebenstein, G. Grioli, S. Haddadin, H. Hoppner, A. Jafari, M. Laffranchi, D. Lefeber, F. Petit, S. Stramigioli, N. Tsagarakis, M. Van Damme, R. Van Ham, L. Visser, and S. Wolf, "Variable impedance actuators: A review," *Robotics and Autonomous Systems*, vol. 61, no. 12, pp. 1601–1614, 2013. [Online]. Available: https://www.sciencedirect.com/science/article/pii/S0921889013001188

[13] G. Grioli, S. Wolf, M. Garabini, M. Catalano, E. Burdet, D. Caldwell, R. Carloni, W. Friedl, M. Grebenstein, M. Laffranchi, D. Lefeber, S. Stramigioli, N. Tsagarakis, M. van Damme, B. Vanderborght, A. Albu-Schaeffer, and A. Bicchi, "Variable stiffness actuators: The user's point of view," *The International Journal of Robotics Research*, vol. 34, no. 6, pp. 727–743, 2015. [Online]. Available: https://doi.org/10.1177/0278364914566515

[14] T. S. Tadele, T. J. de Vries, and S. Stramigioli, "Combining energy and power based safety metrics in controller design for domestic robots," in *2014 IEEE International Conference on Robotics and Automation (ICRA)*. IEEE, 2014, pp. 1209–1214.

[15] G. Raiola, C. A. Cardenas, T. S. Tadele, T. De Vries, and S. Stramigioli, "Development of a safety-and energy-aware impedance controller for collaborative robots," *IEEE Robotics and automation letters*, vol. 3, no. 2, pp. 1237–1244, 2018.

[16] T. Kröger and F. M. Wahl, "Online trajectory generation: Basic concepts for instantaneous reactions to unforeseen events," *IEEE Transactions on Robotics*, vol. 26, no. 1, pp. 94–111, 2009.

[17] V. Magnanimo, S. Walther, L. Tecchia, C. Natale, and T. Guhl, "Safeguarding a mobile manipulator using dynamic safety fields," in *2016 IEEE/RSJ International Conference on Intelligent Robots and Systems (IROS)*. IEEE, 2016, pp. 2972–2977.

[18] A. De Luca, A. Albu-Schaffer, S. Haddadin, and G. Hirzinger, "Collision detection and safe reaction with the dlr-iii lightweight manipulator arm," in *2006 IEEE/RSJ International Conference on Intelligent Robots and Systems*. IEEE, 2006, pp. 1623–1630.

[19] S. Haddadin, A. De Luca, and A. Albu-Schäffer, "Robot collisions: A survey on detection, isolation, and identification," *IEEE Transactions on Robotics*, vol. 33, no. 6, pp. 1292–1312, 2017.

[20] P. Balatti, D. Kanoulas, G. F. Rigano, L. Muratore, N. G. Tsagarakis, and A. Ajoudani, "A self-tuning impedance controller for autonomous robotic manipulation," in *2018 IEEE/RSJ international conference on intelligent robots and systems (IROS)*. IEEE, 2018, pp. 5885–5891.

[21] S. Haddadin, H. Urbanek, S. Parusel, D. Burschka, J. Roßmann, A. Albu-Schäffer, and G. Hirzinger, "Real-time reactive motion generation based on variable attractor dynamics and shaped velocities," in *2010 IEEE/RSJ International Conference on Intelligent Robots and Systems*. IEEE, 2010, pp. 3109–3116.

[22] L. D. Landau and E. M. Lifshitz, *Mechanics, Third Edition: Volume 1 (Course of Theoretical Physics)*, 3rd ed. Butterworth-Heinemann, Jan. 1976.